

Article

Dual-Band 2×1 Monopole Antenna Array and Its MIMO Configuration for WiMAX, Sub-6 GHz, and Sub-7 GHz Applications

Sanaa Iriqat ^{1,*}, Sibel Yenikaya ¹ and Mustafa Secmen ²¹ Department of Electrical and Electronics Engineering, Bursa Uludag University, Bursa 16059, Turkey; sguler@uludag.edu.tr² Department of Electrical and Electronic Engineering, Yasar University, Izmir 35100, Turkey; mustafa.secmen@yasar.edu.tr

* Correspondence: sanairiqat.94@gmail.com

Abstract: This study introduces a cost-effective monopole antenna array and its MIMO configuration. The single element consists of a rectangular patch monopole featuring five circular slots at the center, accompanied by two thin slots at the top, offering a wide bandwidth (2–7.62 GHz) and a peak gain of 3.8 dBi. For gain improvement, a 2×1 antenna array is demonstrated. This antenna array exhibits dual-band behavior; spans from 2 to 3.71 GHz and from 5.9 to 7.54 GHz; covers the 2.5 GHz band (2.3–2.7 GHz), a significant portion of the n78 band (3.3–3.71 GHz), and the n96 band (5.925–7.125 GHz); and is assigned to WiMAX, sub-6 GHz, and sub-7 GHz applications, respectively. The antenna array achieves a peak gain of 6.47 dBi. Lastly, a two-element MIMO configuration derived from the 2×1 array is designed. Implementing a defected ground structure (DGS) on the ground plane plays a crucial role in enhancing the isolation from 7 dB to 20 dB. The presented MIMO antenna covers the desired frequency bands of 2.5 GHz, n78, and n96 with a peak gain of 7.5 dBi and high radiation efficiency (<99%), which qualifies it for WiMAX, sub-6 GHz, and sub-7 GHz applications.



Citation: Iriqat, S.; Yenikaya, S.; Secmen, M. Dual-Band 2×1 Monopole Antenna Array and Its MIMO Configuration for WiMAX, Sub-6 GHz, and Sub-7 GHz Applications. *Electronics* **2024**, *13*, 1502. <https://doi.org/10.3390/electronics13081502>

Academic Editors: Shaoqiu Xiao, Kai-Da Xu, Xiongying Liu and Yi Fan

Received: 25 March 2024

Revised: 9 April 2024

Accepted: 12 April 2024

Published: 15 April 2024



Copyright: © 2024 by the authors. Licensee MDPI, Basel, Switzerland. This article is an open access article distributed under the terms and conditions of the Creative Commons Attribution (CC BY) license (<https://creativecommons.org/licenses/by/4.0/>).

1. Introduction

When the radio was first invented, it stunned the world to realize that individuals in different countries could communicate and hear each other's voices. Since then, advancements and technological progress have continued to develop day after day [1]. Presently, not only can people in one country hear those in another, but they can also visually perceive and interact with them like they were physically together in real time [2]. This remarkable achievement has been made possible by the continuous development of wireless technology [3].

The evolution of successive telecommunication networks (1G–5G) has introduced advances in data rates, capacity, and decreased latency [4]. Presently, 5G technology is expected to interconnect every aspect of our global existence. It will revolutionize several industries, such as healthcare, transportation, agriculture, and more [5]. For sub-6 GHz 5G applications, 5G New Radio includes frequency bands such as n77 (3.3–4.2 GHz), n78 (3.3–3.8 GHz), and n79 (4.4–5.0 GHz). The n96 band, which spans from 5.925 to 7.125 GHz, is classified as sub-7 GHz for applications that operate at frequencies higher than 5 GHz [6]. Compared to mm wave regions, sub-6 GHz and sub-7 GHz frequency bands offer more coverage and lower propagation losses [7]. MIMO technology drives the capabilities of 5G communication, enhancing data transfer rates and spectrum efficiency [8].

Numerous MIMO antenna configurations have been introduced in the literature for 5G sub-6 GHz and 5G sub-7 GHz applications covering diverse frequency ranges, like

LTE band 42 (3.4–3.6 GHz), LTE band 43 (3.6–3.8 GHz), LTE band 46 (5.1–5.8 GHz), n96 (5.925–7.125 GHz), and others. The research detailed in [9] presents a four-element MIMO antenna for 5G applications. To improve isolation between adjacent antennas, a shared grounding branch is employed as a decoupling structure. Operating within the frequency bands of 3.5 GHz and 4.9 GHz, this MIMO antenna provides minimum isolations of 17 dB and 20 dB, respectively. In [10], a four-port, two planar inverted-F antenna (PIFA) element is reported. To achieve spatial diversity, the two antennas are diagonally positioned on opposite sides. The implementation of the defected ground structure technique reduces mutual coupling between the ports by minimizing the current flow between them. This antenna spans a frequency range of approximately 2.7 to 3.6 GHz, with an isolation exceeding 13 dB. The work described in [11] introduces a four-element MIMO antenna designed for 5G cell phone applications. The unit element is composed of a monopole antenna, a planar inverted-F antenna, and a slot implemented using a defected ground structure (DGS). The antennas are positioned at right angles to each other at the corners of the substrate. The MIMO antenna operates between 3.3 and 5.8 GHz, delivering a satisfactory gain of 3.5 to 6 dBi while keeping the isolation level above 15 dB. In [12], a MIMO antenna module designed for fifth-generation smartphones is introduced. The module contains radiating metal strips and two feeding ports. Enhancements of the isolation between ports and between modules include the incorporation of a chip capacitive decoupler and spiral slots. With a minimum isolation of 12 dB, the two ports' measured –6 dB bandwidths are 310 MHz (3.42–3.73 GHz) and 360 MHz (3.33–3.69 GHz), respectively. In [13], a six-element MIMO antenna for 5G sub-6 GHz applications is presented. The single antenna utilizes a loop-type configuration. Two antennas are positioned in the center of the PCB, and four antennas are positioned at the corners for pattern diversity characteristics. The MIMO antenna operates in the 2.38–2.72 GHz and 3.17–3.84 GHz frequency bands, providing a peak gain of 6 dBi, with inter-port isolation exceeding 10 dBi. In [14], an eight-element MIMO antenna for sub-6 GHz and WLAN applications is presented. The MIMO antenna has a bandwidth of 2.7 GHz, specifically ranging from 3.3 to 6 GHz, and a compact size of $72 \times 72 \text{ mm}^2$. To enhance isolation across the desired frequency bands, triangle-shaped slots and a T-shaped stub were utilized. The MIMO antenna achieves more than 2.5 dBi peak gain, with more than 15 dB port-to-port isolation. In [15], a novel MIMO antenna with dual-band capability and four ports is discussed. The antenna has two resonance frequencies of 3.56 GHz and 5.28 GHz with bandwidths of 65 MHz and 112 MHz, and gains of 4.2 dBi and 2.8 dBi, respectively. The MIMO antenna design achieves a minimum inter-element isolation of 22 dB, with dimensions of $90 \times 90 \times 1.57 \text{ mm}^3$.

Previous works in the field have mostly focused on either achieving high bandwidth or optimizing for higher gain, so there is a great need for an antenna design that excels in both aspects concurrently. In this study, a rectangular novel-shaped monopole antenna array and its MIMO configuration are presented. The 2×1 antenna array exhibits dual-band operation, covering the frequency ranges of (2–3.71 GHz) and (5.9–7.54 GHz), thus encompassing the 2.5 GHz, n78, and n96 frequency bands assigned for WiMAX and 5G applications. The array antenna has compact dimensions of $63 \times 50 \text{ mm}^2$ and a peak gain of 6.47 dBi. In contrast, the two-element MIMO antenna demonstrates resonance behavior comparable to that of the antenna array but achieves a higher peak gain of 7.5 dBi. The MIMO antenna configuration proposed in this work exhibits a new and simple geometric structure that distinguishes it from existing complex structures in the literature. In comparison to previously reported works, the antenna design presented herein achieves a distinct performance of both higher gain and broader bandwidth. The MIMO antenna demonstrates a low envelope correlation coefficient (ECC) of less than 0.0002, a minimal channel capacity loss (CCL) of less than 0.1 bps/Hz, a diversity gain (DG) exceeding 9.991 dB, a total active reflection coefficient (TARC) below –10 dB, a mean effective gain (MEG) lower than –6.2 dB, and high radiation efficiency (<99%), making it a suitable option for WiMAX, 5G sub-6 GHz, and 5G sub-7 GHz applications.

2. Antenna Design and Analysis

2.1. Single Antenna Configuration

The single antenna was printed on a Rogers RO4003C (Rogers Corporation, Evergem, Belgium) substrate, which has a thickness of 1.52 mm, a loss tangent of 0.0027, and a relative permittivity of 3.55. Figure 1 shows the proposed antenna design. The overall dimensions of the printed monopole antenna are $25.7 \times 50 \text{ mm}^2$. The initial width and length of the printed monopole in Figure 1 are calculated by Equations (1) and (2):

$$W = \frac{1}{2f_r\sqrt{\mu_0\epsilon_0}} \sqrt{\frac{2}{\epsilon_r + 1}} \quad (1)$$

$$L = \frac{1}{4f_r\sqrt{\epsilon_{ref}}\sqrt{\mu_0\epsilon_0}} \quad (2)$$

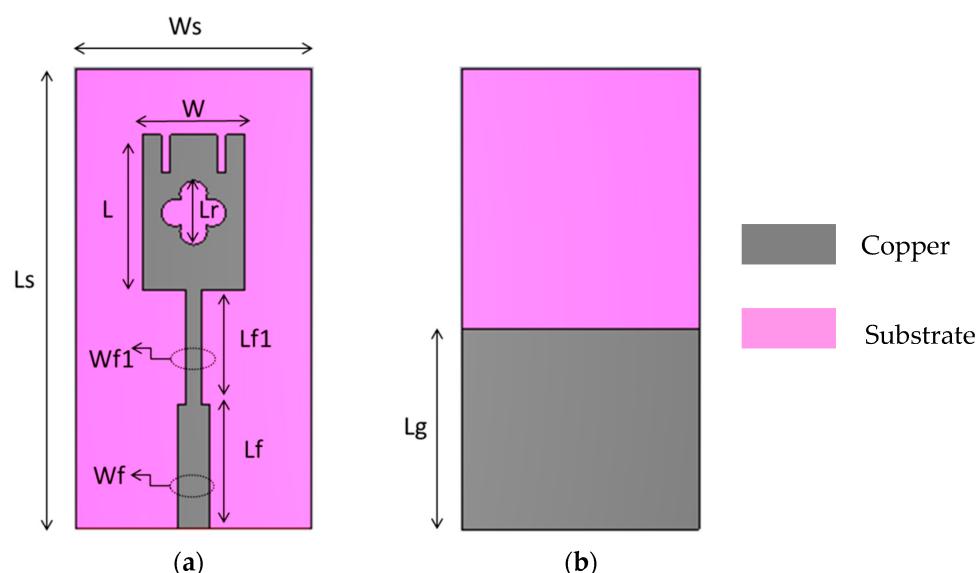


Figure 1. The proposed single-element design: (a) front; (b) back.

The radiating element consists of a rectangular patch with five circular slots (radius = 1.5 mm) forming a rose-shaped slot at the center, along with two thin slots ($1 \times 4 \text{ mm}^2$) at the top of the patch. A 50Ω microstrip feedline with a width of 3.5 mm was used to feed the antenna. Impedance matching between the transmission line and the rectangular patch was accomplished by using a quarter-wavelength transformer with a characteristic impedance of 75 ohm. As displayed in Figure 1, the portion of $L_f1 = 12 \text{ mm}$ that extends 8.5 mm above the ground plane forms the microstrip transmission line. The proposed single-element antenna has a wideband behavior spanning from 2 to 7.62 GHz, which covers most of the frequency bands allocated for WiMAX, sub-6 GHz, and sub-7 GHz applications, as shown in Figure 2.

The design procedure of the antenna can be understood from Figure 3. Different configurations were designed from step 1 to step 3 to improve the antenna's bandwidth, gain, and efficiency. As seen in Figure 3, the rose-shaped slot, along with two thin slots at the top of the monopole patch (step 3), was ultimately chosen as the most effective design for improving antenna performance. The inclusion of these slots led to increased bandwidth and gain in the higher-frequency region, as seen in Figure 3a,b, compared to the other antenna configurations (steps 1 and 2). It is also noted that the addition of these slots effectively contributed to the increase in radiation efficiency in the higher-frequency region, which is attributed to the higher gain achieved in that region, as illustrated in Figure 3c. These improvements show that these slots effectively modify the radiation characteristics of the antenna, leading to enhanced directivity and radiation efficiency at higher frequencies.

It is important to highlight that the thin slots, along with the rose-shaped slot, contributed together to enhancing the antenna's performance. Utilizing only the thin slots did not lead to any performance improvement, whereas employing only the rose-shaped slot resulted in the degradation of antenna performance. However, when both types of slots were used together, they notably enhanced the antenna performance. This improvement was due to the modified surface current distribution induced by the combined effect of the slots. Therefore, only the results for both types of slots used together in the same design were considered and are presented in Figure 3.

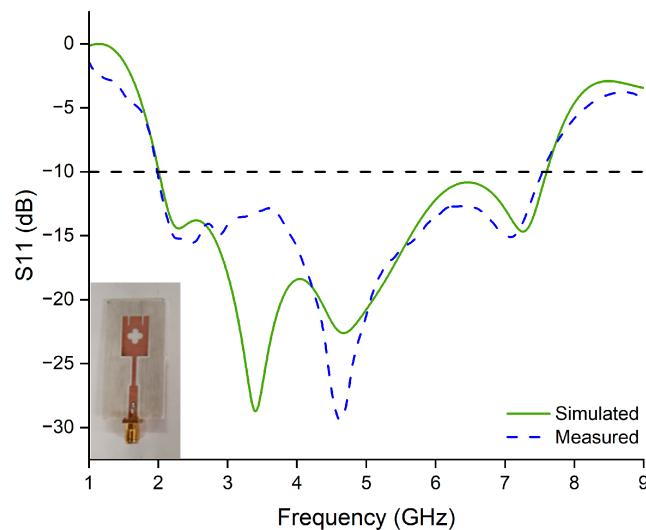
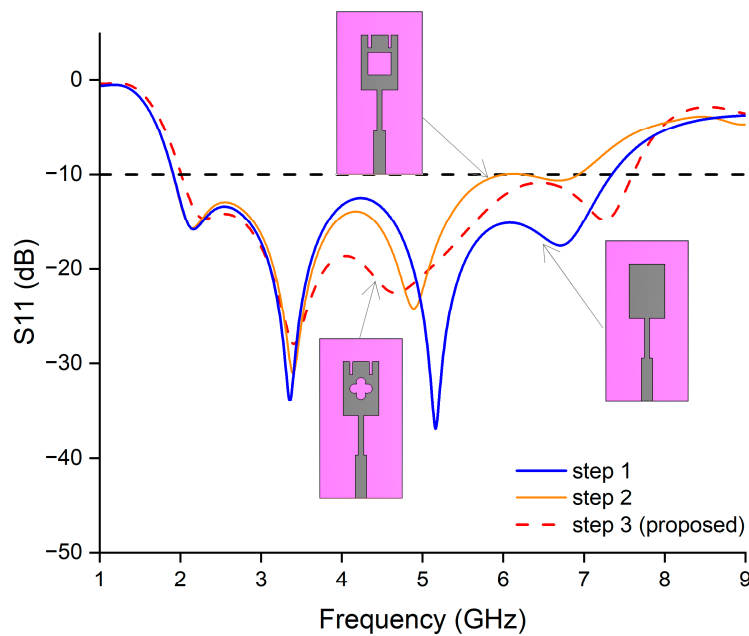
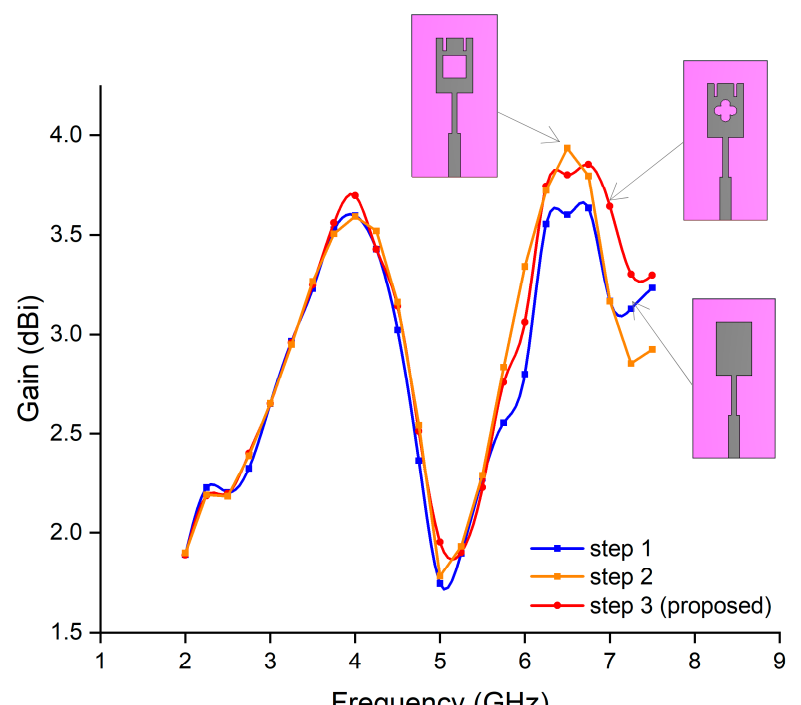


Figure 2. Simulated and measured reflection coefficient of the single antenna.

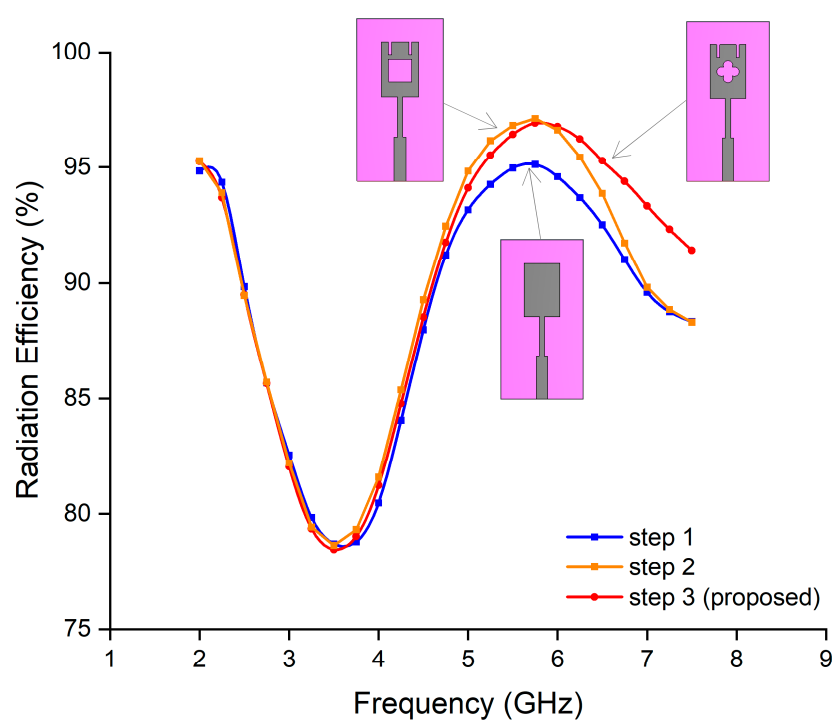


(a)

Figure 3. Cont.



(b)



(c)

Figure 3. Evolution of the single-antenna design: (a) simulated reflection coefficient; (b) simulated realized gain; (c) simulated radiation efficiency.

A crucial parameter that greatly influences the antenna's performance regarding return loss is the length of the ground plane (L_g). For the ground plane to fully cover both the 50 ohm and 75 ohm transmission lines and form a quarter-wave transformer, the maximum value of L_g should be $L_f + L_{f1} = 25.5$ mm. If it exceeds this value, the structure will start to resemble a microstrip patch rather than a printed monopole. Therefore, a maximum of 25 mm was selected for L_g analysis. On the other hand, considering the frequency range of 2–7.62 GHz, the center frequency is approximately 4.8 GHz. For a 75 ohm transmission line at 4.8 GHz, the quarter wavelength is about 9.5 mm. When $L_f = 13.5$ mm is added to this, theoretically, $L_g = 9.5 + 13.5 = 23$ mm can be selected. By performing a parametric sweep around the theoretical value of 23 mm (± 2 mm), the most optimal value of L_g was found to be 22 mm, as shown in Figure 4. This value closely aligns with the theoretical expectation. At $L_g = 22$ mm (proposed), the antenna demonstrates a wideband response spanning from 2 to 7.62 GHz. The adjustment in L_g improves impedance matching. This impedance matching is crucial for maximizing power transfer and, consequently, enhancing radiation efficiency and bandwidth. The design parameters of the single-monopole antenna are provided in Table 1.

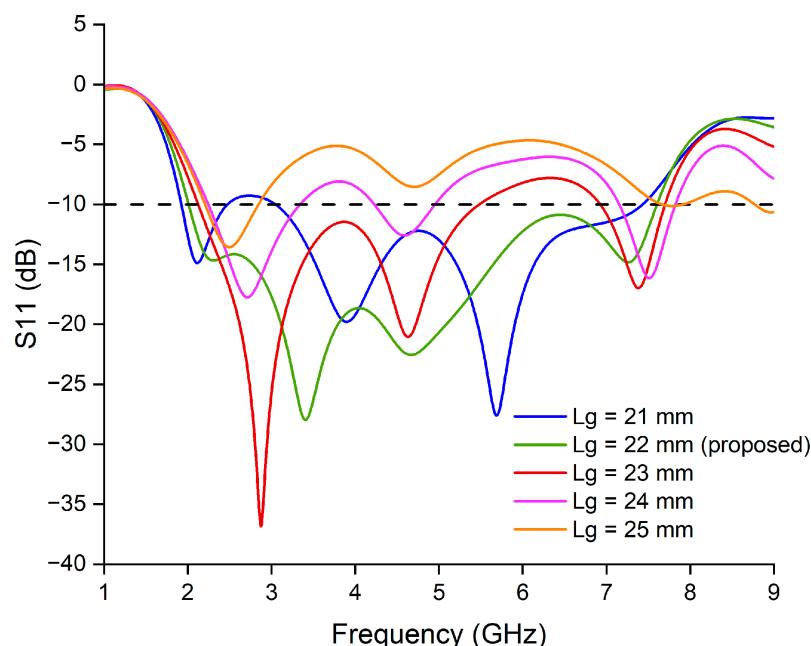


Figure 4. Reflection coefficient variations with different ground plane sizes.

Table 1. Optimal parameters for the final design of the single antenna.

Parameter	Dimension (mm)	Parameter	Dimension (mm)
W_s	25.7	L_s	50
W	11	L	17
W_f	3.5	L_f	13.5
W_{f1}	1.6	L_{f1}	12
L_g	22	L_r	7

2.2. Antenna Array Configuration

Antenna arrays typically provide increased gain compared to a single element, making them suitable for meeting the requirements of 5G technology [16]. A monopole antenna array is a configuration of multiple monopole antennas arranged next to each other. When signals from multiple antennas are combined, they experience constructive or destructive interference depending on their relative phases. The constructive interference results in an increase in signal strength, effectively enhancing the gain of the array in the desired

direction, while destructive interference is used to suppress energy from undesired directions [17]. Thus, to increase the antenna gain, the single element was converted into a linear array consisting of two elements as depicted in Figure 5. The feeding network was designed and optimized to achieve the desired performance. Initially, the monopole antennas were matched to 75 ohm transmission lines. Afterwards, the feed networks of the 2×1 antenna array were combined using a T-junction, enabling the entire array to be matched to a 50 ohm transmission line.

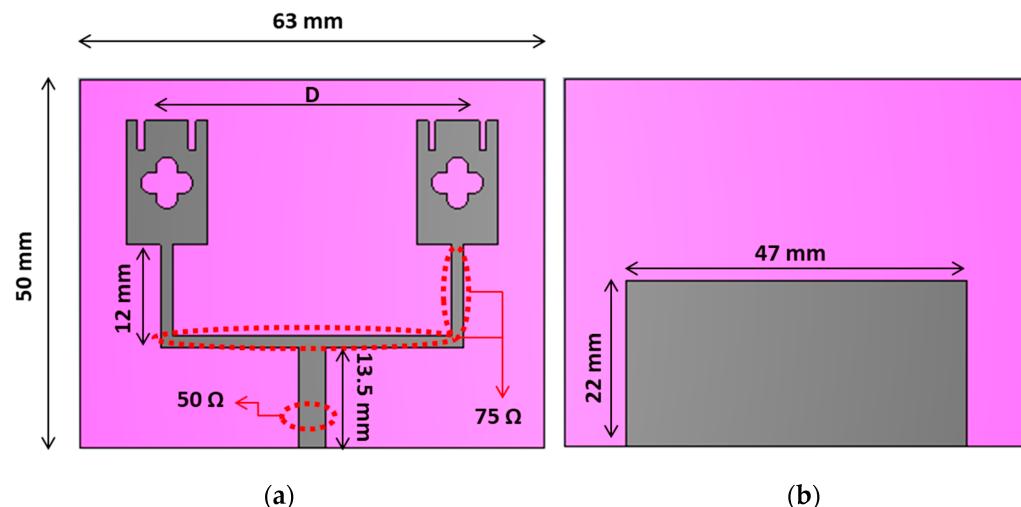


Figure 5. A 2×1 antenna array: (a) front; (b) back.

While the single element has wider band characteristics, the array antenna exhibits dual-band behavior as depicted in Figure 6. According to the -10 dB criteria, the antenna operates within a dual band with bandwidths of 1.71 GHz and 1.63 GHz, spanning from 2 to 3.71 GHz and 5.9 to 7.54 GHz, respectively.

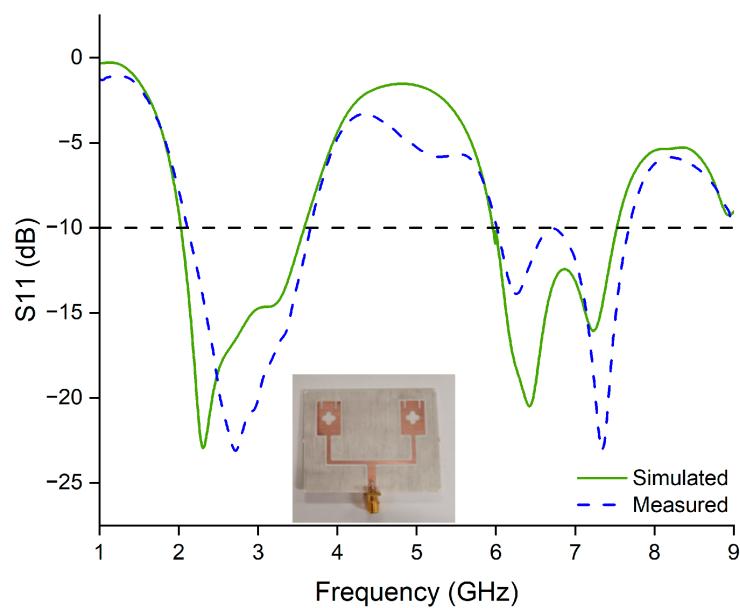
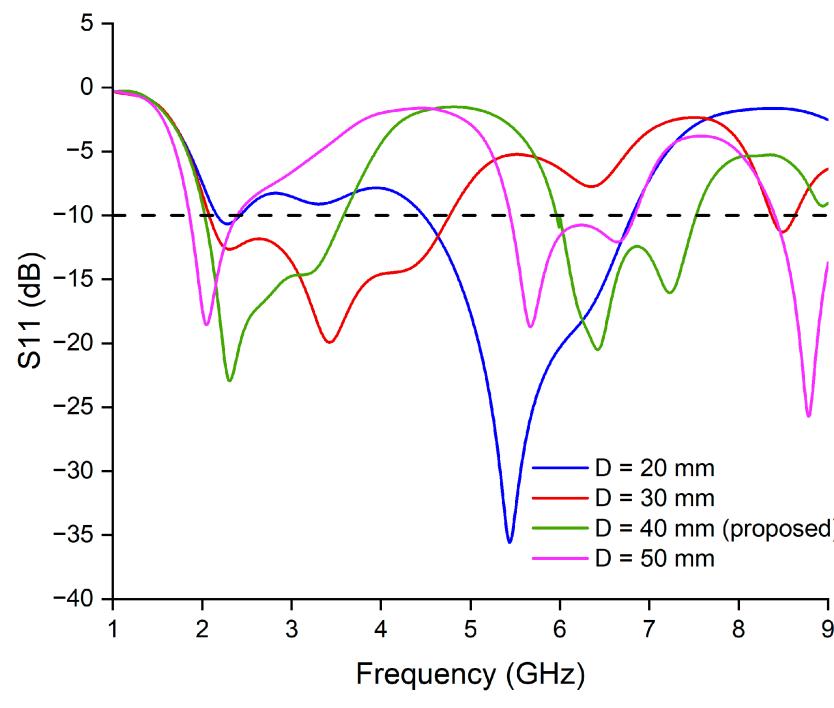


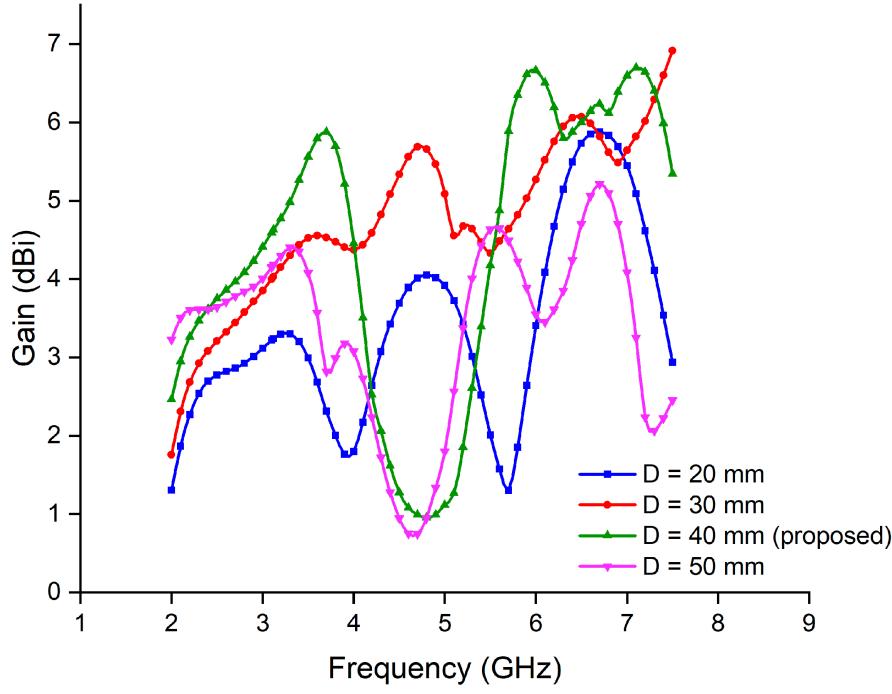
Figure 6. Simulated and measured reflection coefficient (S_{11}) of the array antenna.

The spacing between patches in an antenna array plays a pivotal role in influencing its dual-band behavior, as demonstrated in the analysis depicted in Figure 7. Systematic variation in the spacing (D) from 20 mm to 50 mm was conducted to optimize the antenna

performance across the WiMAX band (2.5 GHz), 5G sub-6 GHz band (n78), and 5G sub-7 GHz band (n96).



(a)



(b)

Figure 7. Effect of patch spacing on (a) reflection coefficient; (b) gain.

At smaller spacing values (e.g., $D = 20$ mm), limited coverage and compromised performance in the desired frequency bands were observed. This is attributed to the strong mutual coupling between adjacent patches, which affects the antenna's impedance

and radiation characteristics, thereby limiting its ability to resonate effectively in the intended bands.

Increasing the spacing (up to $D = 40$ mm) resulted in a notable improvement. At this particular spacing, the intended bands of WiMAX and 5G New Radio (NR) n78 and n96 are covered. Optimal spacing contributed to enhanced isolation between elements, mitigating mutual coupling effects and allowing for independent radiation characteristics in each band. This led to improved resonance and gain across the desired frequency ranges, facilitating reliable operation in both WiMAX and 5G bands, as demonstrated in Figure 7a,b. In the frequency range of 5.9 GHz to 7.5 GHz, the free-space path loss tends to be higher compared to that at lower frequencies. The distance $D = 40$ mm corresponds to 1λ at the highest frequency of 7.5 GHz. Selecting this value ensures that grating lobes will not form across the upper band (5.9–7.5 GHz) for a broadside array configuration. The wavelengths within this range are close to 1λ at 7.5 GHz, allowing the gain of the antenna system to increase due to the array factor. An average gain improvement of 3 dBi was obtained for both operating bands with a peak gain of 6.47 dBi, which is consistent with the theoretical approach [18].

However, with a further increase in spacing ($D = 50$ mm), the total coverage of the intended bands (WiMAX and 5G New Radio (NR) n78 and n96) was lost. Beyond the optimal spacing, the reduction in mutual coupling compromised the antenna's ability to resonate effectively in both bands, leading to reduced gain and inadequate coverage.

2.3. MIMO Configuration

MIMO technology has the capacity to improve communication systems by enhancing link quality, minimizing the impacts of multipath fading, and increasing spectral efficiency [19]. In this section, we extend the 2×1 antenna array to a two-port MIMO antenna with a size of 126×63 mm 2 . Initially, the two antennas were designed in series with a common partial ground plane (109×27 mm 2), as illustrated in Figure 8a. As depicted in Figure 9, the isolation between ports reached 7 dB within the desired bands, which falls far below the acceptable value of 15 dB required for optimal MIMO antenna performance. To enhance the isolation, a rectangular slot was introduced in the middle part of the ground plane, as shown in Figure 8b. By adding this slot, the isolation improved significantly from 7 dB to 20 dB, as demonstrated in Figure 9. The presence of the slot changed the distribution of the electromagnetic fields and disrupted the electromagnetic coupling between antenna elements by modifying the current paths on the ground plane [20]. This modification led to reduced mutual coupling and interference, thus enhancing isolation. For additional insight, a completely separated ground plane structure was employed to examine its impact on isolation, as depicted in Figure 8c. In Figure 9, it is evident that the separated ground planes resulted in decreased isolation in both the lower and upper frequency bands compared to the partial slotted common ground plane. Thus, for better isolation a 16.5×21.3 mm 2 rectangular slot was etched on the ground plane. The width and length of this rectangular slot were carefully optimized to enhance isolation while maintaining dual-band behavior. Since there should be a ground plane under the 75 ohm transmission lines feeding the antennas, the width of the ground plane was ensured to be twice the width of these lines on the sides, and the remaining parts in between were emptied. As the common ground plane contributed to lowering the isolation compared to the separated one, the depth of the slot (21.3 mm) was made as deep as possible without compromising the electrical common ground plane.

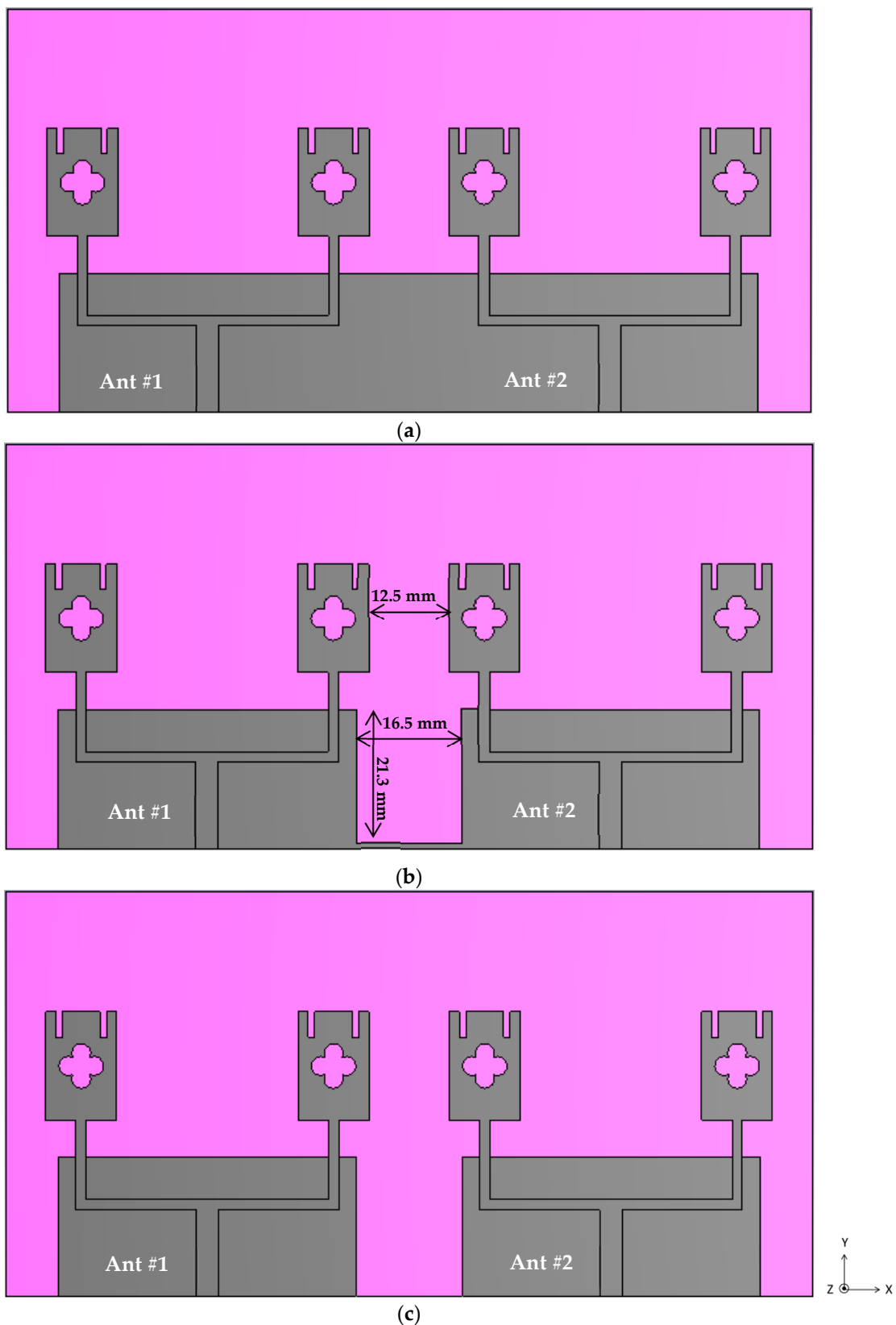


Figure 8. Two-element MIMO antenna design: (a) partial common ground plane; (b) partial slotted common ground plane (proposed); (c) partial separated ground plane.

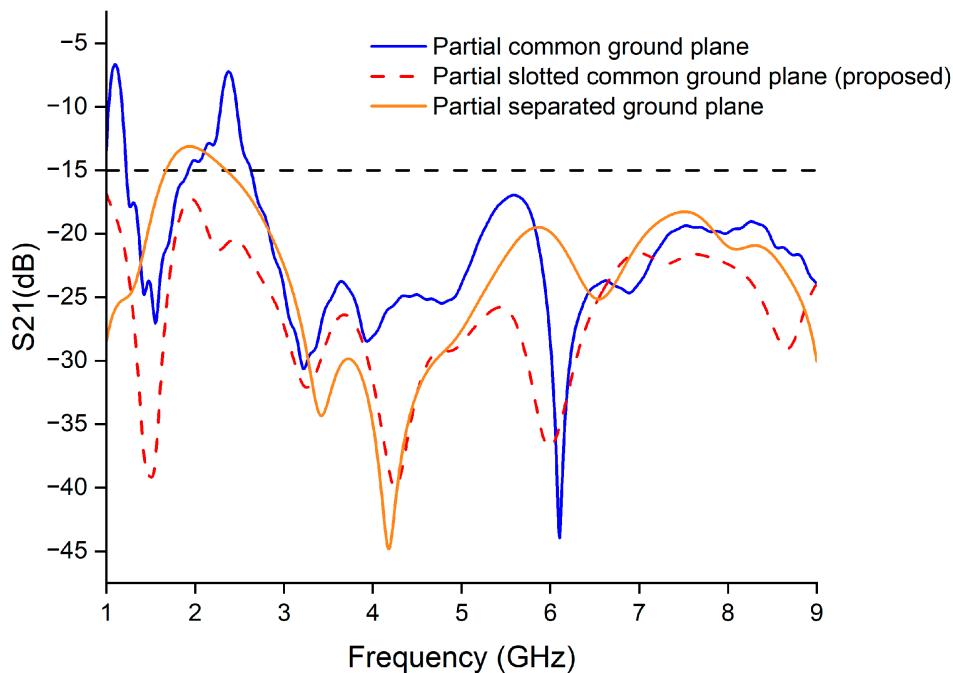


Figure 9. S21 variations with respect to ground plane.

3. Results and Discussion

The proposed antennas were designed in CST Studio Suite V2021 and fabricated by using a PCB milling machine. Figure 10 shows the fabricated two-element MIMO antenna. The measurements were conducted using the MS2028C VNA and radiation pattern measurement setup at Yasar University's Antenna and Microwave Laboratory.

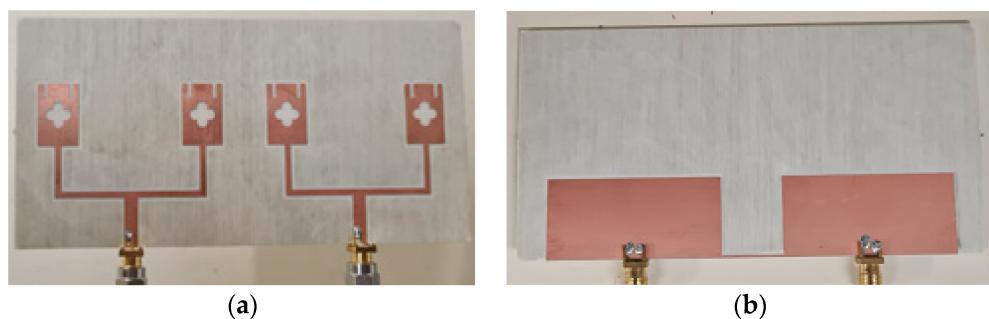


Figure 10. Fabricated MIMO antenna: (a) front; (b) back.

3.1. S-Parameters

The S-parameters of the MIMO antenna, both simulated and measured, are plotted in Figure 11. The proposed MIMO antenna covers dual bands, ranging from 2.1 to 3.6 GHz and 5.9 to 7.4 GHz and encompassing three bands: 2.5 GHz (2.3–2.7 GHz), n78 (3.3–3.6 GHz), and n96 (5.925–7.1 GHz). It was designed for WiMAX, sub-6 GHz, and sub-7 GHz applications. The proposed antenna provides improved isolation exceeding 20 dB between its ports across the operational frequency bands. The simulation and measurement results exhibit good agreement.

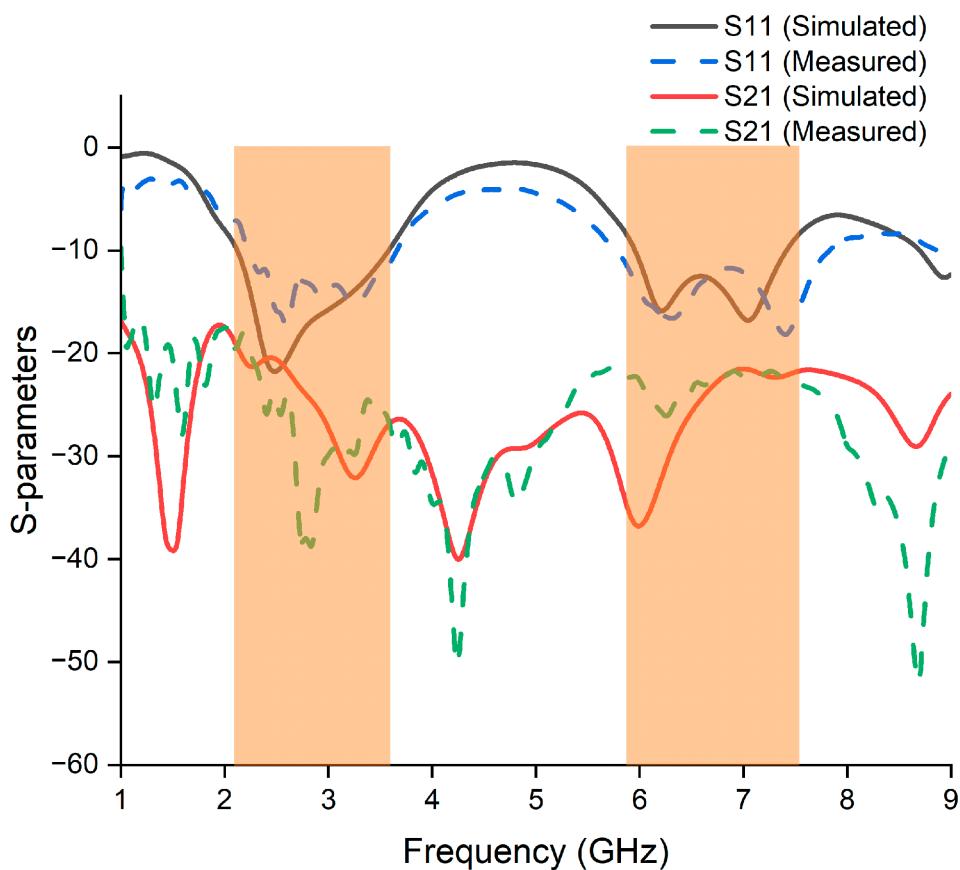


Figure 11. S-parameters of the proposed MIMO antenna.

3.2. Radiation Characteristics

Figure 12 shows the realized gain and radiation efficiency over the frequency of the proposed MIMO antenna. The MIMO antenna exhibits a peak gain of 7.5 dBi, along with a maximum radiation and total efficiency of 99% and 96%, respectively. The gain measurements of the antenna were obtained using a comparison method, where the gain of the antenna was compared to that of a reference antenna with a known gain. An Aaronia Hyperlog 60180 wideband log-periodic antenna (Aaronia, Strickscheid, Germany), which has a gain close to the designed antenna (approximately 5–6 dBi in the relevant frequency range) was selected as the reference antenna. During the measurements, the position of the Aaronia Powerlog 70180 wideband horn antenna, which has a gain of 10–13 dBi within the relevant frequency range, was kept fixed. Each of the MIMO antennas as well as the reference antenna were placed one by one along the broadside direction of the horn antenna, and the gain values of the proposed antenna were determined from the difference in S_{21} (dB) readings on the VNA. The MIMO antenna's two-dimensional (2D) and three-dimensional (3D) radiation patterns at 2.5 GHz and 6.2 GHz are shown in Figure 13. It is noted that the radiation patterns show more directed features at 6.2 GHz compared to the omnidirectional characteristics at 2.5 GHz. This difference can be explained by the upper frequency band's greater gain over the lower frequency band. The simulation results are consistent with the measurements findings.

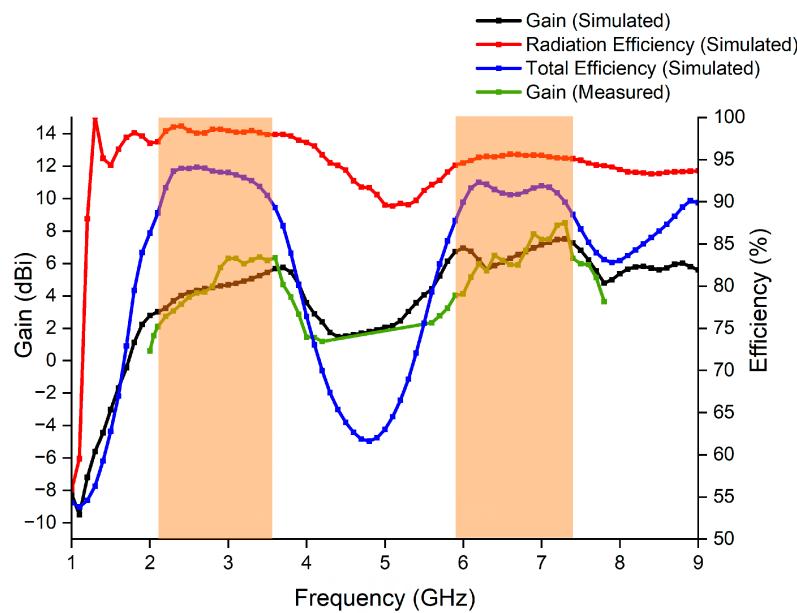


Figure 12. Gain and efficiency variations in the MIMO antenna over the frequency.

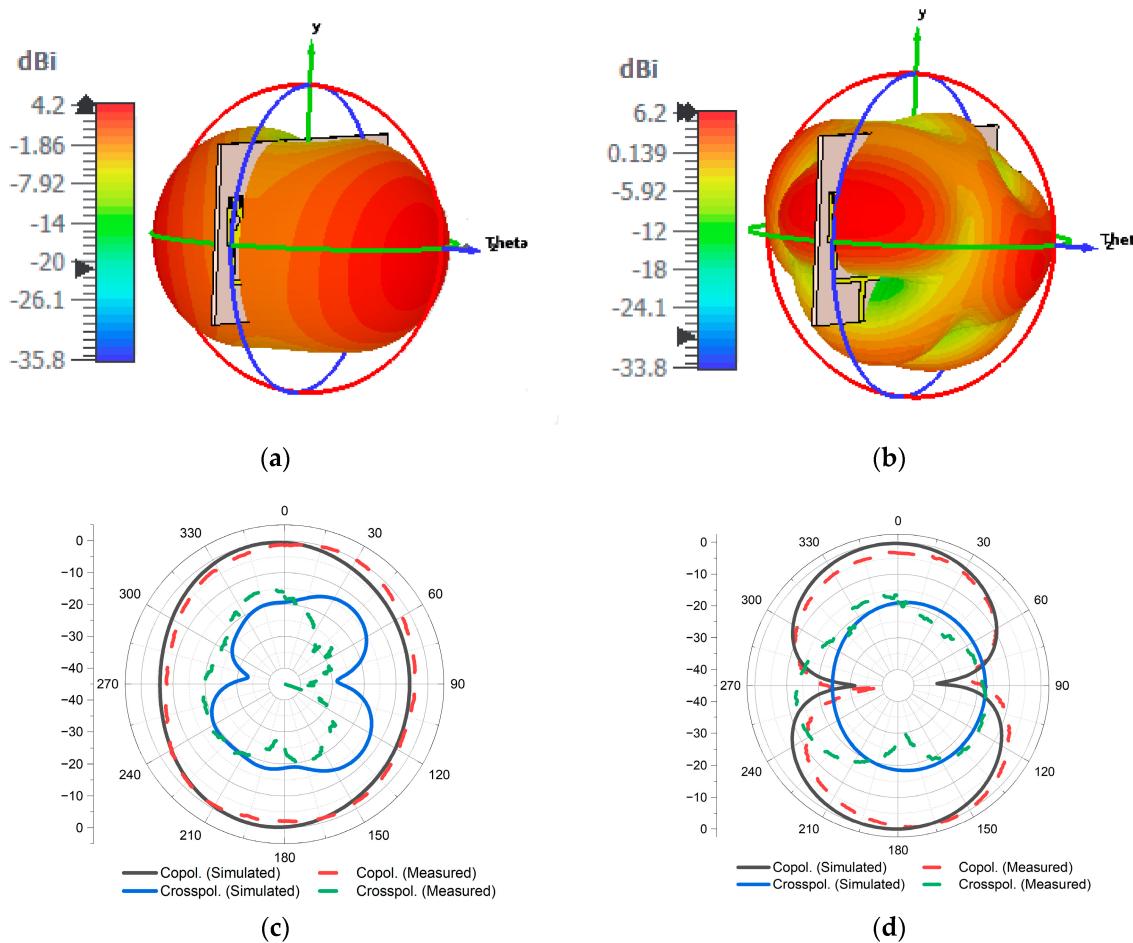


Figure 13. Cont.

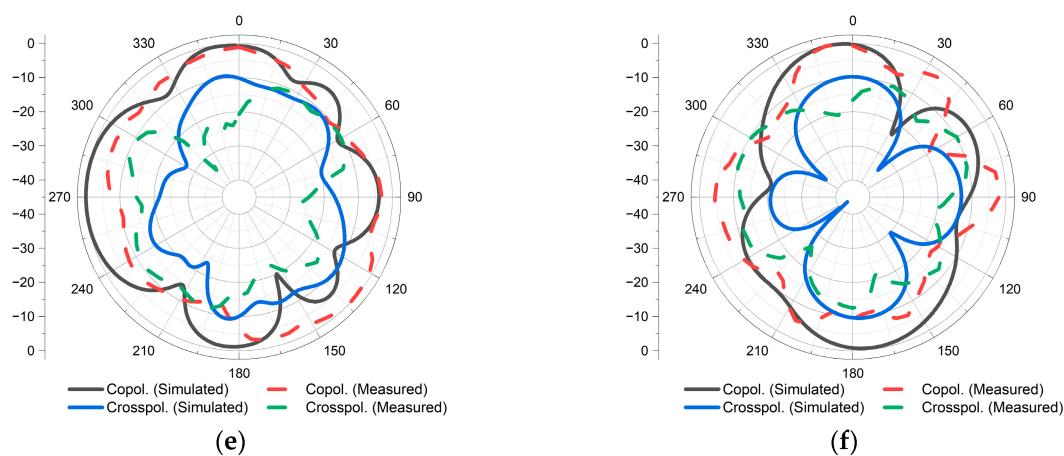


Figure 13. (a) The 3D radiation pattern at 2.5 GHz; (b) 3D radiation pattern at 6.2 GHz; (c) simulated and measured radiation patterns for XZ-plane (H-plane) at 2.5 GHz; (d) simulated and measured radiation patterns for YZ-plane (E-plane) at 2.5 GHz; (e) simulated and measured radiation patterns for XZ-plane (H-plane) at 6.2 GHz; (f) simulated and measured radiation patterns for YZ-plane (E-plane) at 6.2 GHz.

3.3. MIMO Characteristics

One of the main parameters determining how well the antennas are isolated from one another is the envelope correlation coefficient (ECC) [21]. Lower ECC values indicate that the antenna elements are less correlated and more isolated [22]. An ECC value of 0.5 or lower is preferable for better performance [23]. Equations (3) and (4) can be used to calculate the ECC in terms of S-parameters and far-field radiation patterns, respectively.

$$ECC_{s\text{-parameters}} = \frac{|S_{ii} * S_{ij} + S_{ji} * S_{jj}|^2}{(1 - |S_{ii}|^2 - |S_{ij}|^2)(1 - |S_{ji}|^2 - |S_{jj}|^2)} \quad (3)$$

$$ECC_{far\text{-field}} = \frac{\left| \iint_{4\pi} \left[\vec{R}_i(\theta, \varphi) \times \vec{R}_j(\theta, \varphi) \right] d\Omega \right|^2}{\iint_{4\pi} |\vec{R}_i(\theta, \varphi)|^2 d\Omega \iint_{4\pi} |\vec{R}_j(\theta, \varphi)|^2 d\Omega} \quad (4)$$

The reflection coefficient is represented by S_{ii} , while the transmission coefficient is represented by S_{ij} . $\vec{R}_i(\theta, \varphi)$ and $\vec{R}_j(\theta, \varphi)$ denote the three-dimensional radiation patterns of the i th and j th antennas, respectively, and Ω represents the solid angle. As depicted in Figure 14, the recommended MIMO antenna's simulated and measured ECC is extremely low: less than 0.0002 in the desired bands. A low ECC indicates minimal correlation among the signals received by different antenna elements, resulting in higher data rates and improved spectral efficiency.

The diversity gain (DG) parameter measures how effectively the introduction of additional antennas (MIMO antennas) reduces the transmission loss or degradation that can occur in wireless communication due to factors like fading, interference, and attenuation [24,25]. The DG can be calculated by using Equation (5):

$$DG = 10 \sqrt{1 - |ECC_{s\text{-parameters}}|^2} \quad (5)$$

A diversity gain of higher than 9.991 dB is achieved, nearly reaching the optimal value of 10 dB, as shown in Figure 15.

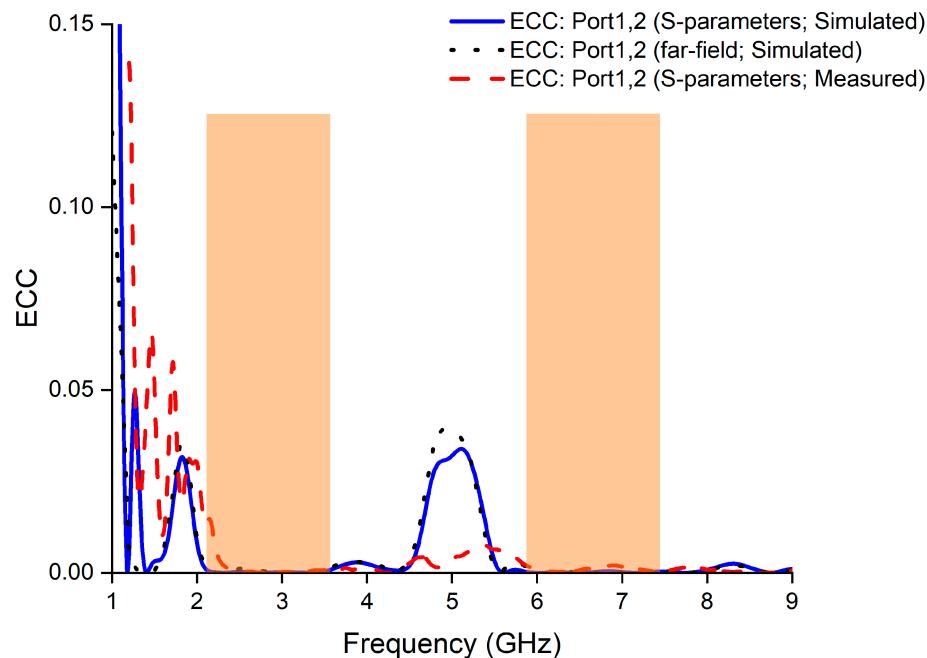


Figure 14. Simulated and measured ECC values of the proposed MIMO antenna.

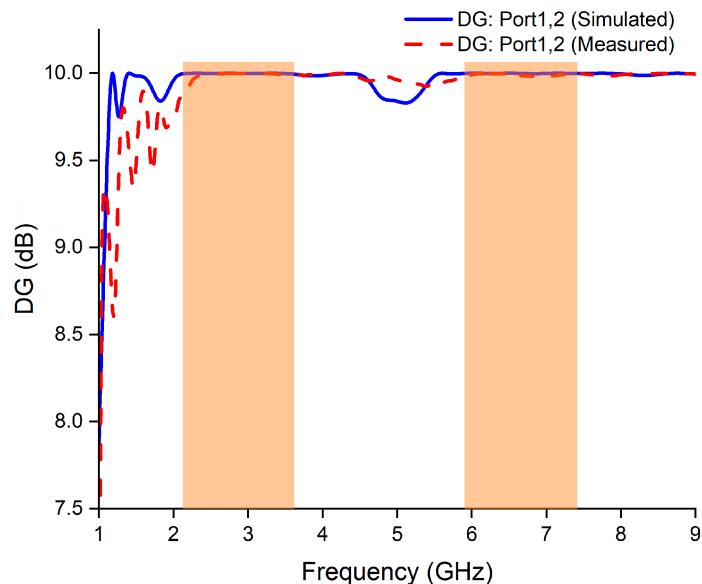


Figure 15. Simulated and measured diversity gain of the proposed MIMO antenna.

A channel capacity loss (CCL) between antenna elements may arise as a result of correlation effects [26]. The formula provided in Equation (6) can be utilized for calculating the CCL:

$$CCL = -\log_2 \left(1 - |S_{ii}|^2 - |S_{ij}|^2 \right) \quad (6)$$

Figure 16 shows that in the desired bands, the simulated and measured values of CCL are less than 0.1 bps/Hz, which is below the acceptable limit of 0.5 bps/Hz [27].

The only parameter employed to determine the unpredictable phase shifts between incoming signals is the total active reflection coefficient (TARC). The TARC is defined as

the square root of the ratio of the total reflected power to the total incident power [28,29]. Equation (7) can be used to determine the TARC based on S-parameters:

$$TARC = \frac{\sqrt{|S_{ii} + S_{ij}e^{j\theta}|^2 + |S_{ji} + S_{ii}e^{j\theta}|^2}}{\sqrt{2}} \quad (7)$$

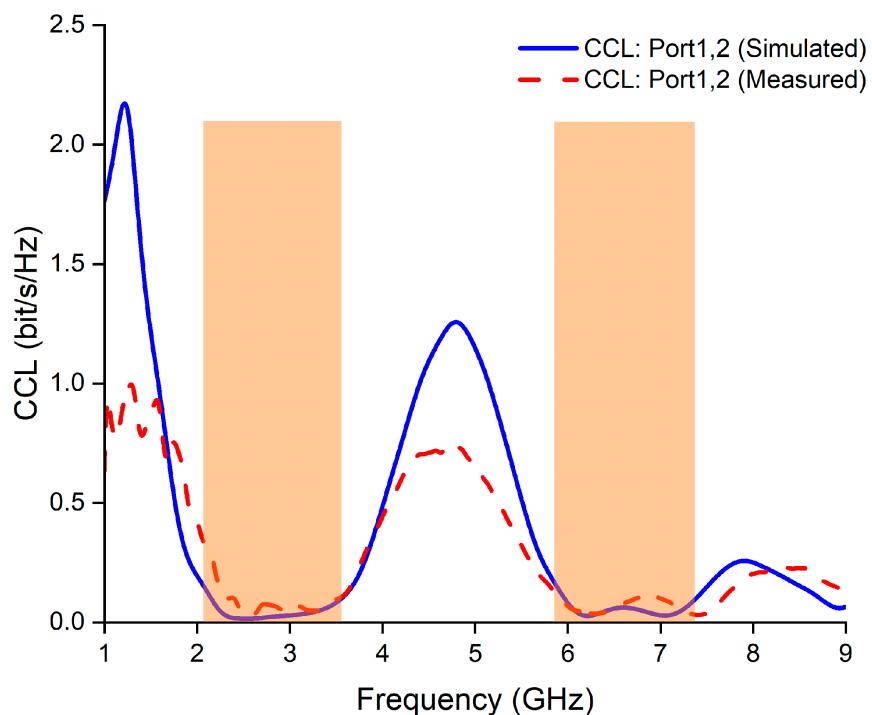


Figure 16. Simulated and measured CCL of the proposed MIMO antenna.

TARCs were obtained for different excitation phases (θ) which vary from 0° to 180° in steps of 30° . Both measured and simulated TARCs for the desired bands are depicted as being less than -10 dB in Figure 17.

The mean effective gain (MEG) serves as a diversity performance parameter that indicates how much more power the MIMO antenna in a multipath environment can receive than the isotropic antenna [30]. The MEG of the proposed antenna can be calculated using Equation (8) [31]:

$$MEG_i = 0.5 \left[1 - \sum_{j=1}^M |S_{ij}| \right] \quad (8)$$

where M stands for the total number of elements within the MIMO system. The values of MEG_1 and MEG_2 can be calculated using the following equations [32]:

$$MEG_1 = 0.5 \left[1 - |S_{11}|^2 - |S_{12}|^2 \right] \quad (9)$$

$$MEG_2 = 0.5 \left[1 - |S_{21}|^2 - |S_{22}|^2 \right] \quad (10)$$

To achieve enhanced MIMO diversity performance, the MEG values should fall within [33]

$$-3 \leq MEG (\text{dB}) < -12 \quad (11)$$

According to Figure 18, the simulated MEG values change between -6.2 dB and -7 dB in the desired bands, which falls within the acceptable range mentioned above.

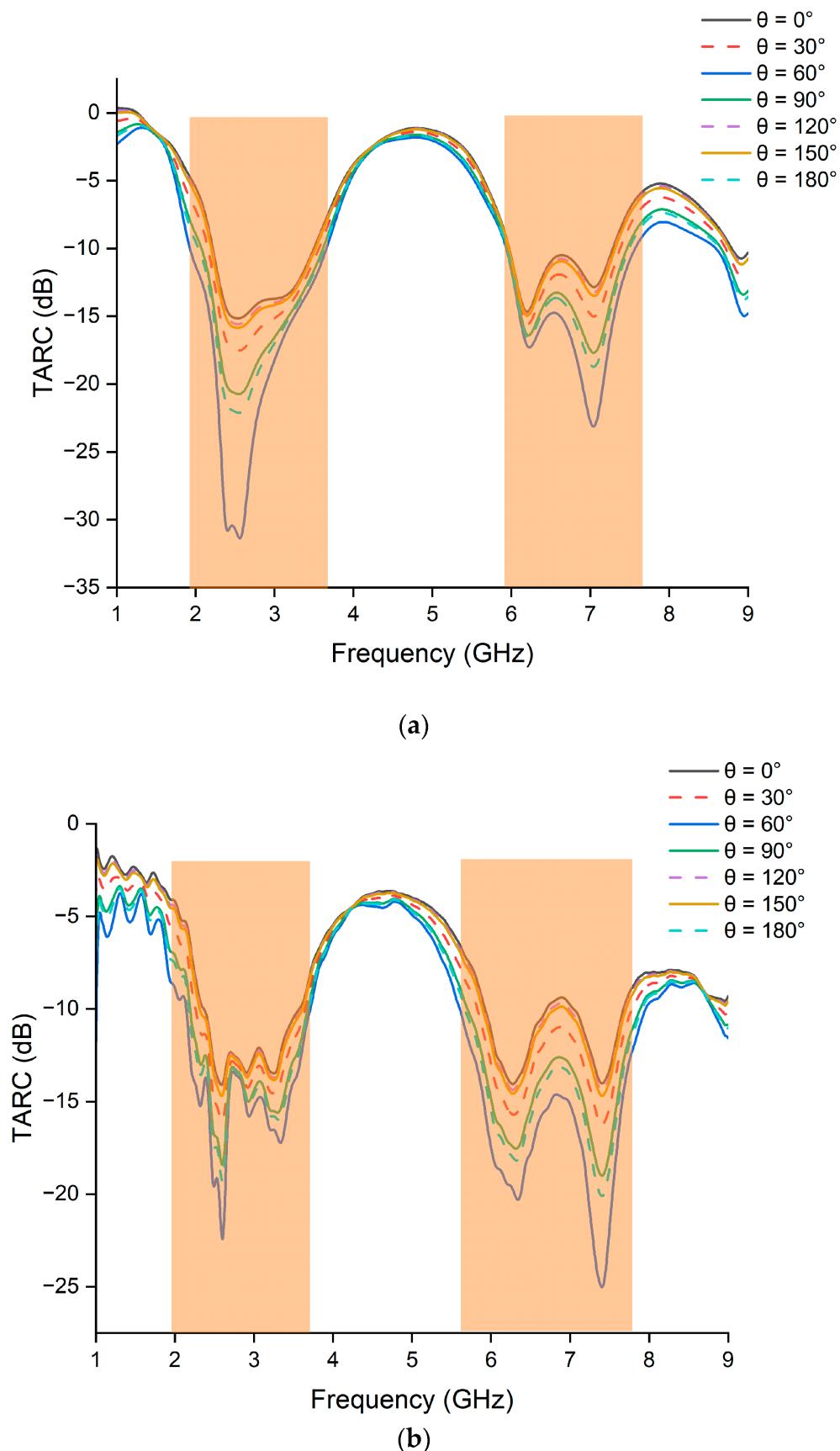


Figure 17. TARC results of the proposed MIMO antenna: (a) simulated; (b) measured.

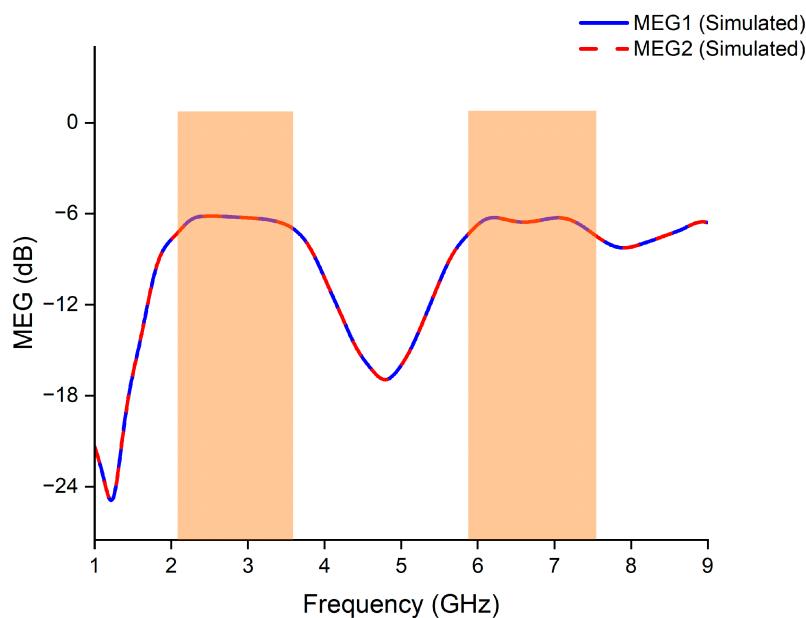


Figure 18. Simulated MEG results of the proposed MIMO antenna.

4. Comparison with Previous Works

Table 2 shows a comparison between the presented MIMO antenna and previous studies. The presented MIMO antenna offers a wider bandwidth, lower mutual coupling, and lower ECC values. Despite the smaller size of the antenna presented in [10], it exhibits lower gain, a narrower bandwidth, and lower isolation compared to the proposed antenna. Moreover, the antenna designs provided in [11,14] demonstrate wide bandwidths, but with lower gain and isolation. Therefore, as mentioned earlier, this antenna provides superior bandwidth and gain, demonstrating better performance and making it the perfect choice for deployment in WiMAX and 5G networks.

Table 2. Comparison of the proposed MIMO antenna with related works.

Ref.	Bandwidth (GHz)	Antenna Dimensions (mm^2)	ECC	Minimum Isolation (dB)	Peak Gain (dBi)
[9]	3.4–3.6, 4.8–5	150 × 75	0.14	17	8
[10]	2.7–3.6	50 × 100	0.009	13	4.5
[11]	3.3–5.8	150 × 75	0.03	15	6
[12]	3.4–3.7	145 × 70	0.01	12	5
[13]	2.38–2.7, 3.19–3.84	150 × 75	0.17	10	6
[14]	3.3–6	72 × 72	0.005	15	>2.5
[15]	3.52–3.6, 5.22–5.38	90 × 90	0.05	22	4.2
Proposed MIMO	2.1–3.6, 5.9–7.4	126 × 63	0.0002	20	7.5

5. Conclusions

In this study, a rectangular antenna with a rose-shaped slot and two thin rectangular slots is presented for WiMAX and 5G applications. The single antenna operates over a wide frequency range (2–7.62 GHz) with a bandwidth of 5.3 GHz and a peak gain of 3.8 dBi. To achieve higher gain, a 2×1 antenna array is demonstrated. The array antenna features dual-band operation. It covers frequencies from 2 to 3.71 GHz with a bandwidth of 1.71 GHz and from 5.9 to 7.54 GHz with a bandwidth of 1.63 GHz, along with a peak gain of 6.47 dBi. Moreover, a two-element MIMO antenna is designed using the proposed antenna array. The dual-band characteristics of the MIMO antenna are very similar to those of the antenna array. The proposed MIMO antenna boasts a peak gain of 7.5 dBi, coupled with an

impressive radiation efficiency that reaches up to 99% and an isolation exceeding 20 dB, making it a strong candidate for WiMAX, 5G sub-6 GHz, and 5G sub-7 GHz applications.

Author Contributions: Conceptualization, S.I., S.Y. and M.S.; methodology, S.I.; software, S.I. and S.Y.; validation, S.Y. and M.S.; formal analysis, S.I.; investigation, S.I., S.Y. and M.S.; resources, S.Y. and M.S.; data curation, S.I., S.Y. and M.S.; writing—original draft preparation, S.I.; writing—review and editing, S.I., S.Y. and M.S.; visualization, S.Y. and M.S. All authors have read and agreed to the published version of the manuscript.

Funding: This research received no external funding.

Data Availability Statement: Data are contained within the article.

Conflicts of Interest: The authors declare no conflicts of interest.

References

- Potter, S.J.; Clayton, D.; Kind-Kovacs, F.; Kuitenbrouwer, V.; Ribeiro, N.; Scales, R.; Stanton, A. *The Wireless World: Global Histories of International Radio Broadcasting*; Oxford University Press: Oxford, UK, 2022.
- Iriqat, S.; Vatansever, F. Comparison of Reality Types. *Uludağ Univ. J. Fac. Eng.* **2020**, *25*, 1155–1168. [\[CrossRef\]](#)
- Solyman, A.; Yahya, K. Evolution of Wireless Communication Networks: From 1G to 6G and Future Perspective. *Int. J. Electr. Comput. Eng.* **2022**, *12*, 3943. [\[CrossRef\]](#)
- Zhou, E.; Cheng, Y.; Chen, F.; Luo, H.; Li, X. Low-Profile High-Gain Wideband Multi-Resonance Microstrip-Slot Antenna with Anisotropic Metasurface. *Prog. Electromagn. Res.* **2022**, *175*, 91–104. [\[CrossRef\]](#)
- Mendonça, S.; Damásio, B.; Freitas, L.; Oliveira, L.; Cichy, M.; Nicita, A. The Rise of 5G Technologies and Systems: A Quantitative Analysis of Knowledge Production. *Telecomm. Policy* **2022**, *46*, 102327. [\[CrossRef\]](#)
- Noor, S.K.; Jusoh, M.; Sabapathy, T.; Rambe, A.H.; Vettikalladi, H.; Albishi, A.M.; Himdi, M. A Patch Antenna with Enhanced Gain and Bandwidth for Sub-6 GHz and Sub-7 GHz 5G Wireless Applications. *Electronics* **2023**, *12*, 2555. [\[CrossRef\]](#)
- Islam, S.; Zada, M.; Yoo, H. Low-Pass Filter Based Integrated 5G Smartphone Antenna for Sub-6-GHz and Mm-Wave Bands. *IEEE Trans. Antennas Propag.* **2021**, *69*, 5424–5436. [\[CrossRef\]](#)
- Jakhar, J.; Jhajharia, T.; Gupta, B. Asymmetric Flare Shape Patch MIMO Antenna for Millimeter Wave 5G Communication Systems. *Prog. Electromagn. Res. C* **2023**, *136*, 75–86. [\[CrossRef\]](#)
- Ren, Z.; Zhao, A. Dual-Band MIMO Antenna with Compact Self-Decoupled Antenna Pairs for 5G Mobile Applications. *IEEE Access* **2019**, *7*, 82288–82296. [\[CrossRef\]](#)
- Chattha, H.T. 4-Port 2-Element MIMO Antenna for 5G Portable Applications. *IEEE Access* **2019**, *7*, 96516–96520. [\[CrossRef\]](#)
- Zheng, Z.; Ntawangaheza, J.D.; Sun, L. Wideband MIMO Antenna System for Sub-6 GHz Cell Phone. In Proceedings of the 2021 International Conference on Electronics, Circuits and Information Engineering (ECIE), Zhengzhou, China, 22–24 January 2021; pp. 1–5. [\[CrossRef\]](#)
- Ye, Y.; Zhao, X.; Wang, J. Compact High-Isolated MIMO Antenna Module with Chip Capacitive Decoupler for 5G Mobile Terminals. *IEEE Antennas Wirel. Propag. Lett.* **2022**, *21*, 928–932. [\[CrossRef\]](#)
- Al-Bawri, S.; Islam, M.; Singh, M.; Alyan, E.; Jusoh, M.; Sabapathy, T.; Padmanathan, S.; Hossain, K. Broadband Sub-6GHz Slot-Based MIMO Antenna for 5G NR Bands Mobile Applications. *J. Phys. Conf. Ser.* **2021**, *1962*, 12038. [\[CrossRef\]](#)
- Addepalli, T.; Kumar, M.S.; Jetti, C.R.; Gollamudi, N.K.; Kumar, B.K.; Kulkarni, J. Fractal Loaded, Novel, and Compact Two- and Eight-Element High Diversity MIMO Antenna for 5G Sub-6 GHz (N77/N78 and N79) and WLAN Applications, Verified with TCM Analysis. *Electronics* **2023**, *12*, 952. [\[CrossRef\]](#)
- Upadhyaya, T.; Sorathiya, V.; Al-shathri, S.; El-Shafai, W.; Patel, U.; Pandya, K.V.; Armghan, A. Quad-Port MIMO Antenna with High Isolation Characteristics for Sub 6-GHz 5G NR Communication. *Sci. Rep.* **2023**, *13*, 19088. [\[CrossRef\]](#) [\[PubMed\]](#)
- Hsieh, R.; Chu, F.-C.; Ho, C.-Y.; Wang, C.-C. Advanced Thin-Profile Fan-Out with Beamforming Verification for 5G Wideband Antenna. In Proceedings of the 2019 IEEE 69th Electronic Components and Technology Conference (ECTC), Las Vegas, NV, USA, 28–31 May 2019; pp. 977–982. [\[CrossRef\]](#)
- Bangash, K.; Ali, M.M.; Maab, H.; Ahmed, H. Design of a Millimeter Wave Microstrip Patch Antenna and Its Array for 5G Applications. In Proceedings of the 2019 International Conference on Electrical, Communication, and Computer Engineering (ICECCE), Swat, Pakistan, 24–25 July 2019; pp. 1–6. [\[CrossRef\]](#)
- Malviya, L.; Gupta, P. Millimeter Wave High-Gain Antenna Array for Wireless Applications. *IETE J. Res.* **2023**, *69*, 2645–2654. [\[CrossRef\]](#)
- Mistri, R.K.; Mahto, S.K.; Singh, A.K.; Sinha, R.; Al-Gburi, A.J.A.; Alghamdi, T.A.H.; Alathbah, M. Quad Element MIMO Antenna for C, X, Ku, and Ka-Band Applications. *Sensors* **2023**, *23*, 8563. [\[CrossRef\]](#)
- Zambak, M.F.; Al-Bawri, S.S.; Jusoh, M.; Rambe, A.H.; Vettikalladi, H.; Albishi, A.M.; Himdi, M. A Compact 2.4 GHz L-Shaped Microstrip Patch Antenna for ISM-Band Internet of Things (IoT) Applications. *Electronics* **2023**, *12*, 2149. [\[CrossRef\]](#)
- Nirmal, S.; Kumar, S.; Chandel, R. High Isolation Compact Two Port 5G MIMO Diversity Antenna with Asymmetrical Feed and Partial Ground Structure. *Prog. Electromagn. Res. C* **2023**, *136*, 23–36. [\[CrossRef\]](#)

22. Addepalli, T.; Anitha, V.R. Design and Analysis of a Novel Compact Spanner-Shaped Ultra-Wideband Antenna for MIMO Systems. *Int. J. Commun. Syst.* **2021**, *34*, e4739. [[CrossRef](#)]
23. Musaed, A.; Al-Bawri, S.; Abdulkawi, W.; Aljaloud, K.; Yusoff, Z.; Islam, M. High Isolation 16-Port Massive MIMO Antenna Based Negative Index Metamaterial for 5G Mm-Wave Applications. *Sci. Rep.* **2024**, *14*, 290. [[CrossRef](#)]
24. Zahra, H.; Awan, W.A.; Ali, W.A.E.; Hussain, N.; Abbas, S.M.; Mukhopadhyay, S. A 28 GHz Broadband Helical Inspired End-Fire Antenna and Its MIMO Configuration for 5G Pattern Diversity Applications. *Electronics* **2021**, *10*, 405. [[CrossRef](#)]
25. Baz, A.; Jansari, D.; Lavadiya, S.; Patel, S.K. Miniaturized and High Gain Circularly Slotted 4×4 MIMO Antenna with Diversity Performance Analysis for 5G/Wi-Fi/WLAN Wireless Communication Applications. *Results Eng.* **2023**, *20*, 101505. [[CrossRef](#)]
26. Dey, S.; Dey, S.; Koul, S.K. Isolation Improvement of MIMO Antenna Using Novel EBG and Hair-Pin Shaped DGS at 5G Millimeter Wave Band. *IEEE Access* **2021**, *9*, 162820–162834. [[CrossRef](#)]
27. Pradeep, P.; Jaya Sankar, K.; Paidimarry, C. A Compact Semi-Circular Slot MIMO Antenna with Enhanced Isolation for Sub-6 GHz 5G WLAN Applications. *Wirel. Pers. Commun.* **2022**, *125*, 3683–3698. [[CrossRef](#)]
28. Abbas, M.A.; Allam, A.; Gaafar, A.; Elhennawy, H.M.; Sree, M.F.A. Compact UWB MIMO Antenna for 5G Millimeter-Wave Applications. *Sensors* **2023**, *23*, 2702. [[CrossRef](#)] [[PubMed](#)]
29. Raheel, K.; Ahmad, A.; Khan, S.; Shah, S.A.A.; Ali Shah, I.; Dalarsson, M. Design and Performance Evaluation of Orthogonally Polarized Corporate Feed MIMO Antenna Array for Next-Generation Communication System. *IEEE Access* **2024**, *12*, 30382–30397. [[CrossRef](#)]
30. Yamina, T.; Bensid, C.; Sayad, D.; Mekki, S.; Zegadi, R.; Bouknia, M.; Elfergani, I.; Singh, P.; Rodriguez, J.; Zebiri, C. Low-Profile UWB-MIMO Antenna System with Enhanced Isolation Using Parasitic Elements and Metamaterial Integration. *Electronics* **2023**, *12*, 4852. [[CrossRef](#)]
31. Tangirala, G.; Garikipati, S.; Meshram, M.; Durbhakula, M.; Sharma, V. Quad Element Luna-Shaped UWB-MIMO Antenna with Improved Isolation and Gain Using Novel Decoupling Networks. *Wirel. Netw.* **2024**, *1–13*. [[CrossRef](#)]
32. Shankar Das, G.; Bikash Chamuah, B.; Beria, Y.; Protim Kalita, P.; Buragohain, A. Compact Four Elements SUB-6 GHz MIMO Antenna for 5G Applications. *Mater. Today Proc.* **2023**, *in press*. [[CrossRef](#)]
33. Elabd, R.; Al-Gburi, A. Super-Compact 28/38 GHz 4-Port MIMO Antenna Using Metamaterial-Inspired EBG Structure with SAR Analysis for 5G Cellular Devices. *J. Infrared Millim. Terahertz Waves* **2023**, *45*, 35–65. [[CrossRef](#)]

Disclaimer/Publisher’s Note: The statements, opinions and data contained in all publications are solely those of the individual author(s) and contributor(s) and not of MDPI and/or the editor(s). MDPI and/or the editor(s) disclaim responsibility for any injury to people or property resulting from any ideas, methods, instructions or products referred to in the content.